International Journal of Power Electronics and Drive System (IJPEDS)
Vol. 17, No. 3, September 2026, pp. 1859~1872
ISSN: 2088-8694, DOI: 10.11591/ijpeds.v17.i3.pp1859-1872

Design and simulation of a four-port buck-boost converter integrated with a PID controller for solar power systems

M. S. Mukundaswamy[1,2], Smitha Elsa Peter[3]
[1]PRIST University, Thanjavur, India
[2]Embedded Department of Electrical and Electronics Engineering, Dr. Ambedkar Institute of Technology (Dr. AIT), Karnataka, India
[3]Department of Electronics and Communication Engineering, PRIST University, Thanjavur, India

Article Info

Article history:

Received Mar 17, 2025
Revised Nov 24, 2025
Accepted Dec 11, 2025

Keywords:

Battery
Four-port bidirectional buck-boost converter
Grid
PI controller
PV system

ABSTRACT

This manuscript proposes a bidirectional four-port buck–boost converter for integrating renewable energy sources into a DC microgrid. The proposed topology utilizes a reduced number of components compared to conventional bidirectional multi-port converters, leading to enhanced efficiency and compactness. The converter incorporates bidirectional battery and DC-link ports, making it well-suited for DC microgrid applications that demand coordinated system-level power management. It is capable of interfacing simultaneously with a wind turbine, photovoltaic (PV) panel, battery bank, and DC load. Zero-voltage switching (ZVS) is achieved under steady-state operating conditions, while the converter's dynamic performance is assessed during transient variations in energy sources and load conditions. The efficacy of the proposed method is validated through MATLAB/Simulink simulations.

Corresponding Author:

M. S. Mukundaswamy
PRIST University
Thanjavur, Tamil Nadu, India
Email: mukundswamyms.ee@drait.edu.in

1. INTRODUCTION

The multiport DC-DC converters have attracted so much interest due to the ability to combine various sources of energy and storage with versatile power flow regulation. A more simplified topology of a multiport converter, using just four power switches, has been reported, which allows each source to be independently controlled and two-way power transfer. An experimental prototype was used to verify the feasibility of the proposed PWM and phase-shift methods of independently controlling two output ports [1]. There have been efforts to consider integrated wind solar energy storage plants, which prove to be better than single wind or solar systems in their generation profile. These hybrid designs increase the efficiency of the transmission infrastructure, as well as making the total cost of the plant less than the equivalent generation capacity [2].

Several research efforts have aimed to minimize the number of components as well as enhance soft-switching in multiport converters. It was suggested to have a fully soft-switched 3-port converter that uses fewer active devices with a very simple modulation scheme that does not require optimization or complicated control. An experimental check was made on a 200 W prototype based on PowerSim simulations [3]. Topologies resonant-frequency operated have been designed to provide an easier implementation of the digital control at the cost of providing soft switching of most switches and diodes, like in LLC resonant converters, which are conservative. The efficiency of this type of design was shown with a prototype of 500 W with its maximum output current of 1.25 A [4].

Four-port DC–DC converters have been extensively explored for hybrid renewable energy systems (RES). An integrated four-port converter designed for standalone wind–solar systems was introduced, offering a simpler topology capable of interfacing sources with diverse voltage and current characteristics [5]. Compact and efficient unidirectional non-isolated DC–DC converters with reduced circuit elements have also been reported, capable of operating in multiple modes with minimal control complexity using a single controller set [6]. A four-port converter integrating a PV module and a battery into a bipolar DC microgrid (MG) was proposed, achieving single-phase energy conversion and operating under three distinct modes based on energy management requirements [7].

High-power and high-gain multiport converters have been developed for hybrid energy storage appliances. A current-fed dual active bridge-based multiport converter providing galvanic isolation between the battery and DC bus was validated using a 1 kW prototype [8]. Similarly, a bipolar DC–DC converter combining a multiport dual active bridge with a neutral-point-clamped topology was implemented to integrate renewable sources of varying capacities into a bipolar medium-voltage DC micro grid [9]. Parallel coordination control strategies using isolated multiport converters have been proposed to replace conventional buck–boost circuits, enabling electrical isolation for energy storage micro-sources [10]. Controllers for regulating battery voltage and current while managing bidirectional power flow among wind turbines, PV panels, batteries, and DC micro grids have also been demonstrated [11]. Additionally, isolated three-port DC–DC converters based on series resonant and dual active bridge topologies have been developed for electric vehicle charging stations, supporting both fast and slow charging modes [12].

Buck–boost converters remain a fundamental solution for voltage regulation due to their ability to step up or step-down output voltage. PWM control has been done using microcontrollers to ensure that the output is regulated [13]. In order to enhance dynamic operation, PID, fuzzy, and hybrid fuzzy-PID controllers have been explored in solar-battery buck-boost systems, successfully decreasing the overshoot and oscillations [14]. Extensive analysis of performance trade-offs between controller tuning approaches based on time-domain and frequency-domain analysis has also been pointed out in the literature [15]. Fixed-point digital filter architecture-based digital controllers have also been used (where reprogramming can be accomplished without drastic hardware adaptation). Buck and boost mode closed-loop control have been tested on MATLAB/Simulink with different operating conditions [16]. The dynamic response of unidirectional and bidirectional buck boost converters has been studied, and the refined transient response and low overshoot are realized using PID controllers [17].

More sophisticated modeling and control techniques have been developed to add to converter efficacy. Generalized state-space averaging models (GSSAM) have been used to multiphase interleaved buck converters, especially when the system is oscillating or has high amounts of ripple in the currents [18]. Gating pulse generation strategies using feedback and determining the range of the cycle of duty have been adopted to control the input resistance and stable operation [19]. Active power factor correction (PFC) has also been extensively used in boost converters in both continuous and discontinuous conduction modes [20]. Variable switching frequency methods are suggested to decrease discontinuous conduction at both line voltage zero crossings and minimize switching loss in both voltage peaks to a minimum [21]. PID-controlled PFC boost converters have been applied to enhance the DC voltage regulation [22], and adaptive PWM-based methods have been applied to ensure the minimization of overall harmonic distortion (THD) and stable operation in the closed-loop [23]. Closed-loop control strategies have also shown great reduction in overshoot and efficiency [24]. Mechanisms to enhance power factor and lower THD in AC to DC converters with PID-controlled boost converters have also reported [25]. In-depth analysis of PFC techniques identifies their capabilities as driving input current and minimizing harmonics, and the performance of PFC techniques has been compared to each duty ratio and voltage level [26].

2. METHOD

Figure 1 shows how power interacts to give the photovoltaic (PV) panel and the DC voltage source the ability to feed energy to the DC grid. In order to supply power to the DC grid during periods of renewable energy production, the bidirectional converter is utilized in boost mode while simultaneously charging the battery. An MPPT technique called perturb and observe (P&O) is used to extract the PV panel's maximum power. In case of a reduction of the solar irradiation and the PV power is not enough to meet the demand of the grid, a deficit of power will be compensated by the battery, which feeds the DC grid. In this case, the solution moves to voltage mode control as opposed to MPPT. In the event that both the PV source and the DC voltage source are unavailable, the battery becomes the sole power source for the DC grid. The converter operates in buck mode in this operating condition to be able to control battery charging and discharging.

Charging is resumed when the battery state of charge (SoC) becomes less than a predetermined value, by using the available renewable energy sources. When the sun is not available or not available at all, the battery keeps on discharging to keep the DC-link voltage constant and guarantee continuous power to the grid. The general layout of the system and control approach is presented in the schematic plan revealed in Figure 1.

2.1. Circuit diagram of the proposed system

Figure 2 displays the circuit scheme of the proposed approach. The converter is a four-port bidirectional converter that connects solar modules and a DC source (Ports 1 and 2) on the input side, a battery on Port 3, and a DC grid/load on Port 4 [27]. The circuit uses a solar panel as the main source of energy, and an auxiliary source of DC is supplied to allow the circuit to continue during periods of unavailability of the solar panel. The use of MPPT is done in order to optimize the use of solar irradiance. A bidirectional transformer that is used in amplification mode is used to unite the power sources and provide energy to the DC grid/load. A method of perturb and observer (P&O) is implemented in order to bring the solar module to its maximum power so that the solar module can be easily and directly connected to the DC grid.

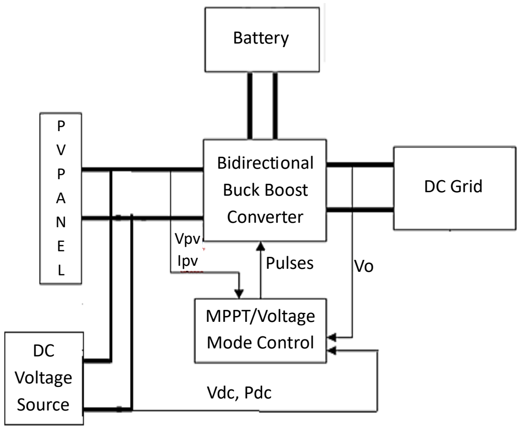

Figure 1. Proposed system

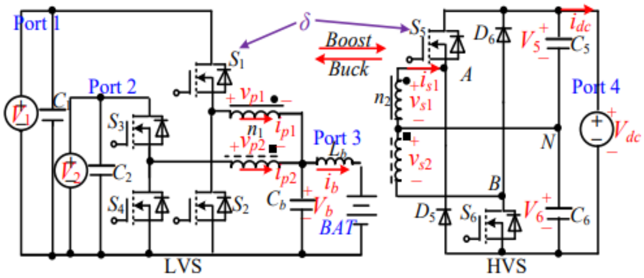

Figure 2. Circuit diagram of the proposed method

2.2. Control strategy scenarios of the proposed converter

Different power-flow conditions between the battery, DC link, and renewable energy source are used to categorize the proposed converter's operation. These operating scenarios ensure proper energy management under varying generation and load conditions. Four distinct scenarios are defined to describe the converter behavior and corresponding operating modes, which is given as follows:

- Scenario 1: P_{dc}<0. When the DC-link power is negative, the converter operates in buck mode, and the battery is charged by absorbing energy from the DC link (Mode 1). If renewable energy power P_{RES}>0, the converter transitions to Mode 2.
- Scenario 2: $p_{RES} > P_{DC}$> 0. In this condition, renewable energy generation exceeds the DC-link power demand. The excess renewable energy is directed to charge the battery, enabling energy storage. Consequently, the converter operates in Modes 2 and 3.
- Scenario 3: $p_{DC} > p_{RES}$. When the available renewable energy is insufficient to meet the DC-link load demand, the battery supplies the power deficit. Under this scenario, the converter operates in Modes 3 and 4 to ensure uninterrupted power delivery.
- Scenario 4: $p_{RES} > 0$ and $p_{DC} > 0$. In the absence of renewable energy generation, the battery becomes the sole energy source supplying the DC link. In this operating condition, only Mode 4 is active.

The DC bus voltage control loop generates the reference current for the inner current control loop, which subsequently determines the duty ratio D, as illustrated in Figure 3. Based on the duty ratio and the availability of solar irradiation, the corresponding delay angle is generated to regulate power flow. Furthermore, a perturb and observe (P&O)-based maximum power point tracking (MPPT) algorithm is employed to ensure maximum power extraction from the solar source under varying irradiation conditions.

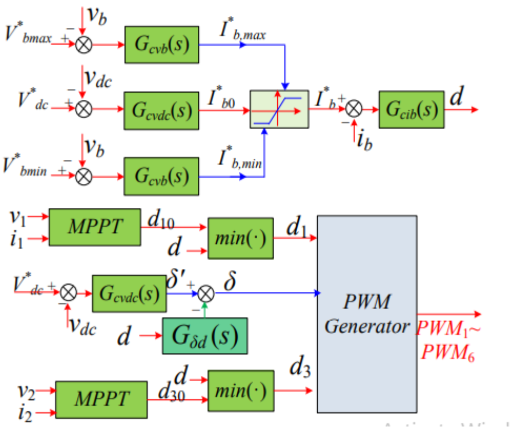

Figure 3. Control strategy of the proposed converter

3. MAXIMUM POWER POINT TRACKING

This section describes the MPPT and control framework implemented in the proposed converter system to achieve efficient power extraction and stable operation. The P&O algorithm adopted for MPPT is illustrated through the flowchart shown in Figure 4. The design of the parameters of the proposed converter, the proportional-integral controlled boost converter, and the PI controllers employed for voltage and current regulation are presented and discussed as follows:

3.1. Design the parameters of the proposed converter

The design of the four-port bidirectional buck–boost converter is carried out to meet both port-level voltage requirements and the DC bus/load reference voltage of the system [28]. The converter input voltage is $\mathrm{V_{in}} = 36\,V$, and the port-level output voltage is $\mathrm{V_o} = 90\,V$. The switching frequency is set to $f_s = 50\,kHz$, and the rated output power is $P = 100\,W$ The system-level DC bus voltage, maintained by the PID controller, is defined as $\mathrm{V}^*_{dc} = 180\,V$. It should be noted that Vdc* is the system-level reference voltage, whereas Vo is utilized for port-level computations.

The duty ratio for the buck-boost converter is calculated as (1).

$$D = \left(\frac{V_o}{V_o - V_{in}}\right) \tag{1}$$

The inductor is designed to limit the ripple current, which is chosen as 20% of the output current, as given in (2).

$$\Delta I_L = 0.2 \times \left(\frac{V_o}{V_{in}}\right) \times I_0 \tag{2}$$

Where the output current I_0 is assumed to be 0.56 A (corresponding to 100 W at the port-level voltage). Using this ripple current, the inductor value is computed as (3).

$$\text{Inductor} \quad L = \left(\frac{V_{in} - D}{\Delta I_L - f_s}\right) \tag{3}$$

The output capacitor is selected to limit voltage ripple, which is set to 2% of the DC bus reference voltage (4).

$$\Delta V_c = 0.02 \times \mathrm{V}^*_{dc} \tag{4}$$

The required capacitance is then calculated as (5).

$$C_o = \frac{\Delta I_L}{8 \times f_s \times \Delta V_c} = \frac{0.28}{8.50 \times 10^3 \times 3.6} \approx 3.375\mu F \tag{5}$$

The designed parameters of the converter are summarized as follows: duty ratio $D = 0.6$, inductor $L = 0.54\,mH$, inductor ripple current $\Delta I_L = 0.28\,A$, output capacitor $C_o = 3.375$ μF, capacitor ripple voltage $\Delta V_c = 3.6\,V$, and system-level DC bus reference voltage $V_{dc}^* = 180\,V$. This design ensures the converter meets both component-level and system-level performance requirements, providing stable and efficient operation under varying load and renewable source conditions.

3.2. Proportional-integral controlled with a boost converter

In this system, gating pulses for the boost converter switch Q are generated using a proportional–integral (PI) controller [29]. The voltage tracking relationship is employed within the voltage control loop to regulate the output voltage of the boost converter, as illustrated in Figure 4. The reference DC voltage (V_{dc}^*) serves as the desired setpoint for the converter output. The difference between this reference voltage and the actual output voltage V_{dc} generates the voltage error V_E, which is then processed by the PI controller to produce the reference control voltage, as shown in (6).

$$V_{dc}^* = k_p \times \omega^* \quad (6)$$

The voltage error is mathematically defined as the difference between the reference and measured DC voltages (V_{dc}). This error signal is continuously evaluated to determine the corrective action required by the controller. The voltage error (V_E) equation is given as (7).

$$V_E = V_{dc}^* - V_{dc} \quad (7)$$

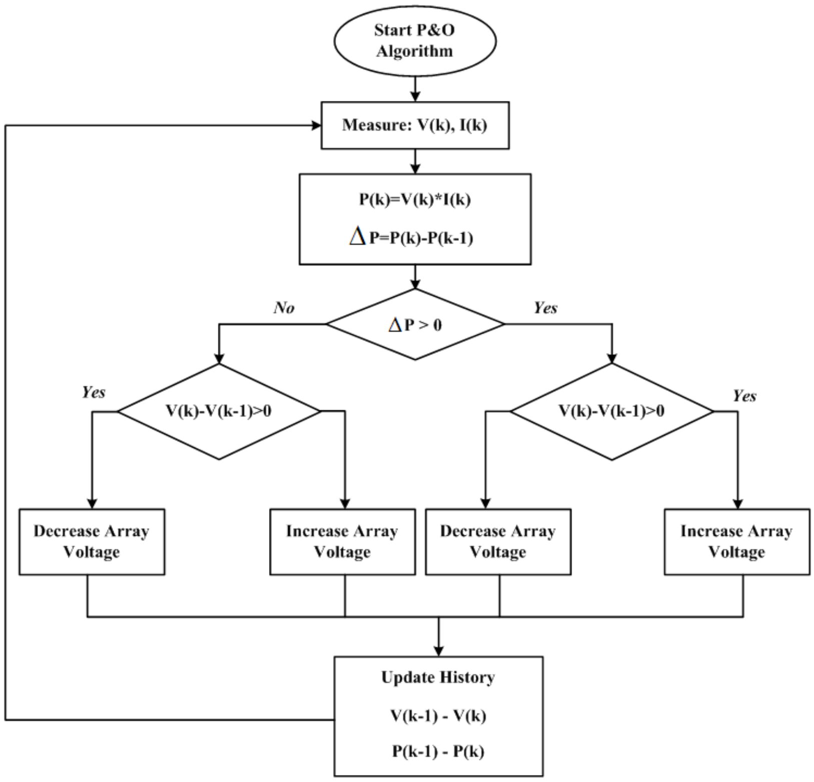

Figure 4. Flowchart for the P&O algorithm of MPPT

The PI controller processes the voltage error to generate the reference-controlled voltage V_C, which governs the switching behavior of the boost converter. The discrete-time PI control law incorporates both proportional and integral actions to reduce steady-state error and improve voltage regulation. The controller equations are expressed as (8) and (9):

$$V_C(k) = V_C(k-1) + K_P \quad (8)$$

$$\{V_E(k) - V_E(k-1)\} + K_I V_E(k) \quad (9)$$

Here, k denotes the current sampling instant, while K_P and K_I represents the proportional and integral gains, respectively. The output of the PI controller is compared with a high-frequency triangular carrier signal M_C to generate the gating pulses for the boost converter switch Q. When $M_C<V_C$, the switch is turned ON (pulse HIGH), and when $M_C \geq$, the switch is turned OFF (pulse LOW), thereby regulating the converter output voltage effectively.

3.3. PI controllers

Proportional-integral (PI) controllers find broad use in control systems in which very fast dynamic response is not a key consideration. These controllers are also the most appropriate when dealing with systems that have disturbances, noise, and parameter changes. Also, PI controllers are effective in systems where there is a large storage of energy, like inductors and capacitors, and dynamic behavior is inherently slower.

The omission of the derivative (D) term removes the complexity of the controller structure and enhances robustness in noisy environments. With these systems, the need for rapid transient response is not always necessary, and tolerable delays of system response can be accepted. Consequently, PI controllers are often used in power electronic converters in steady operating or slowly varying conditions. The primary benefit of a PI controller is that it allows the removal of steady-state error, which cannot be completely removed with a proportional controller alone. This, however, comes at the expense of lower response speed and possible stability constraints. Since it lacks predictive capability, PI controllers cannot suppress oscillations, nor can they reduce the rise time that can cause an overshoot about the reference set point.

The output of the proportional controller is directly related to the instantaneous error signal and is expressed as (10).

$$\text{(P) Controller output} = e(t) \times 100 \,/\, (k_p) \tag{10}$$

Where, $e(t)$ is the instantaneous voltage or current error (i.e., the difference between the reference and measured signal) and k_p is the proportional gain that scales the controller response to the error magnitude. The integral controller output is expressed as (11).

$$\text{Controller output} = \frac{1}{\text{Critical time}} * (\text{critical of } e(t)) \tag{11}$$

Here, the integral term accumulates the error over time, correcting steady-state deviations. The critical time determines the speed of the integral action, controlling how quickly the accumulated error influences the controller output. Together, these actions enable the PI controller to maintain stable DC bus voltage or output current under varying operating conditions.

4. SIMULATION MODEL OF PROPOSED SYSTEM

The proposed system's imitation method is portrayed in Figure 5. In this setup, the DC source and the photovoltaic (PV) panel are connected to the system for t = 1.5 s before being disconnected. From t=0 to t = 1 s, the PV provides power to the load at an irradiation level of 1000 W/m^2, which is lowered to 400 W/m^2 between t = 1 s and t = 1.5 s before disconnection. PV power is used to first charge the battery. The battery enters discharge mode and gives power to the load at t = 1.5 s after the PV source is cut off. The MPPT control approach produces gating pulses for the converter during the PV-connected interval. Following PV disconnection, the converter receives the necessary pulses from t = 1.5 to t = 2 s using a solo control scheme.

During operation, the six switches (S1-S6) coordinate the power flow between the PV panel, auxiliary DC source, battery, and load. When S1 is ON, energy from the PV panel is stored in the inductor L, enabling the buck operation and charging the battery if its voltage is below the supply voltage. When S4 is ON, the stored energy in the inductor is released, acting as a source and providing feedback to the battery through the body diode while simultaneously supplying the load. If S1 is OFF, S3 is ON, and S4 is OFF, energy flows from the PV panel and inductor to the battery, while the transformer secondary is energized, transferring power to the load. S2 controls the auxiliary DC source, allowing it to supply power when the PV source is insufficient, and S5 and S6 manage bidirectional operation with the transformer, ensuring energy can flow from the converter to the load or from the load back to the battery as needed. This coordinated switching sequence ensures efficient energy transfer from all sources to the battery and load, maintaining proper buck-boost operation and continuous power delivery under varying operating conditions.

In the full-bridge half-controlled converter, a voltage-controlled strategy is employed. The reference DC voltage is set to 180 V and is compared with the measured load voltage. Both signals are converted to per-unit values and applied to the PID controller. Based on the resulting voltage error, the PID controller generates the duty ratio, which is supplied to the pulse generator to produce the gating signals. A voltage control loop is used to limit the battery voltage. When the battery voltage exceeds the reference value, the load-based PID controller regulates the duty ratio within predefined upper and lower limits. If the battery voltage is below the reference value, the duty ratio is adjusted accordingly to maintain voltage regulation. This approach forms a dual conditional control loop in which the duty ratio selection depends on the operating voltage conditions.

The duty ratio limits are defined based on the battery operating voltage range, with a lower limit corresponding to 24 V and an upper limit corresponding to 38 V. In addition, a battery-based current control loop is implemented to generate the reference current. The reference battery current is compared with the measured battery current, and the resulting error is processed by a PID controller to generate a duty ratio. This duty ratio is then compared with the duty ratio obtained from the MPPT algorithm, and the minimum of the two is selected to ensure safe and stable operation. The selected duty ratio is finally applied to the pulse generator to produce the gating signals for the converter switches. The duty ratio for Source 1 is shown in Figure 8, while the duty ratio at the secondary side of Source 2, where the secondary voltage varies, is presented in Figure 9.

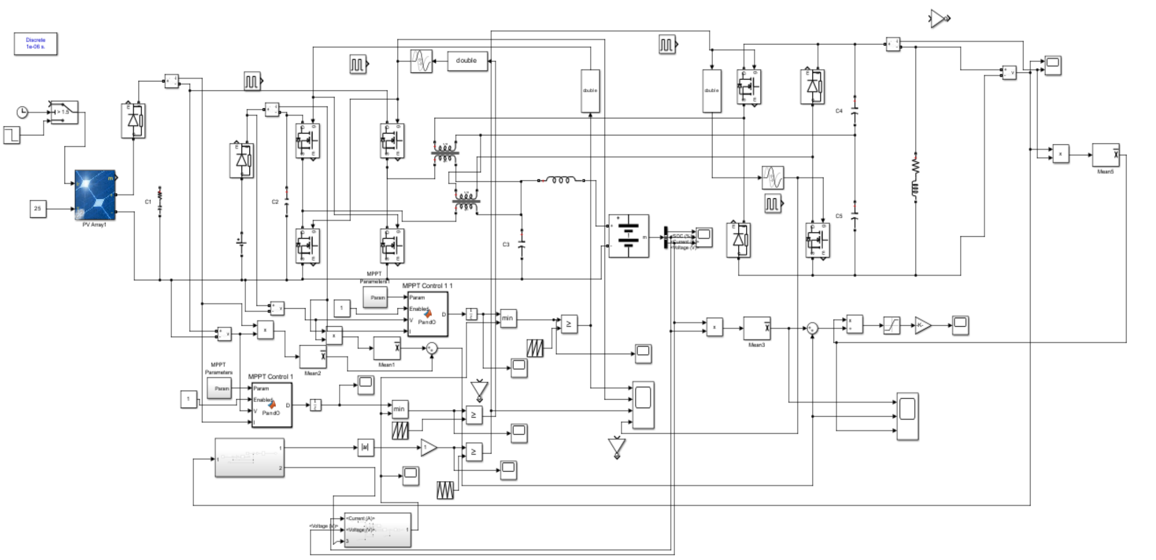

Figure 5. Simulation model of the proposed method

4.1. Calculated the RL load values for different power factors

The RL load parameters were calculated for different power factor scenarios to evaluate the performance of the proposed converter under varying load conditions. The calculations consider both the active power PPP and the reactive power *Q*, which determine the equivalent resistance *R* and inductance *L* of the load. The voltage across the load is assumed to be constant at the system nominal value *V*, and the supply frequency is *f*. The formulas used for the calculations are given in (12) and (13).

$$Resistance\ (R) = \frac{V^2}{P} \tag{12}$$

$$Inductance\ (L) = \frac{V^2}{Q*2*\pi*f} \tag{13}$$

- Case (a): Power factor = 0.9

For an active power of $P = 4500\,W$ and a reactive power of $Q = 500\,VAR$, the equivalent resistance and inductance are calculated using the above expressions. The resulting values are:

$$R = 7.2\,\Omega, \quad L = 0.2\,H$$

This configuration represents a predominantly resistive load with minimal reactive component.

- Case (b): Power factor = 0.8

For a load with $P = 4000\ W$ and $Q = 1000\ VAR$, the calculated resistance and inductance are:

$$R = 8.1\ \Omega, \quad L = 0.1\ H$$

In this scenario, the reactive component is higher than in Case (a), resulting in a lower inductance to maintain the required reactive power.

- Case (c): Power factor = 0.7

For a more reactive load with $P = 3500\, W$ and $Q = 1500\, VAR$, the corresponding load parameters are:

$$R = 9.26\Omega, \quad L = 0.069H$$

This case represents a highly inductive load, which is important for evaluating converter performance under low power factor conditions. These calculations provide a basis for simulating and analyzing the dynamic and steady-state behavior of the proposed converter with different load characteristics. They ensure that both resistive and inductive effects are properly considered, enabling accurate assessment of voltage regulation, current sharing, and efficiency under realistic operating conditions.

5. RESULTS AND DISCUSSION

This segment demonstrates the output response of the PID-controlled bidirectional buck–boost converter (BBC). The BBC operates in two modes, namely buck mode and boost mode. The experimental outcomes are attained using MATLAB/Simulink. The output responses of different system models are analyzed and presented below.

Figure 6 presents the load voltage and current under different operating modes. It illustrates the voltage response during PV power generation at various irradiation levels, including both battery charging and discharging conditions. The voltage waveform settles at approximately 0.0415 s, reaching a steady-state value of 178.3 V. The corresponding battery charging and discharging performance is further represented by the state-of-charge (%SoC) waveforms.

Figure 7 displays the state of charge (SoC) corresponding to the PV-generated voltage and current. Initially, when the PV system generates power, the battery operates in charging mode, resulting in an increase in the %SoC. When the PV source is disconnected, the battery begins to discharge, leading to a decrease in the %SoC.

The changes in the duty ratio of the proposed converter due to changes in irradiation of the PV are provided in Figure 8. PV is off, power to both battery and load. In this, until t = 0.3 s, PV is supplying power to both the battery as well as load. After t = 0.3 s, the irradiation is reduced, but still, PV is providing a supply to the battery as well as the load. At t = 0.5 s, the battery starts to discharge.

The power curves, like Input power, battery power, and load power is provided in Figure 9, the power curves of battery and load. In this initially battery was charging with battery power of around 350 W, and at t = 0.5 s, the battery began to discharge and provide energy to the load. The load is changed from 2 kW to 5 kW along with the source, and the battery of 24 V is replaced with 48 V. The load voltage and current waveforms are provided in Figure 10. Figure 10 gives the discussion of the load voltage and current depending on the load condition. The load power is varied to 5 kW instead of 2 kW, and the battery voltage is varied to 48 V instead of 24 V. In spite of these differences, the load voltage is regulated very well in relation to the reference value and shows strong dynamic performance.

The results of the analysis of battery voltage and current at the time of charge and discharge are presented in Figure 11. When charging, the battery voltage is kept within the specified operating range of 24 V to 38 V, and the current changes gradually when discharging to aid the load, which proves that battery operations are safe and stable. The analysis of the converter efficiency when on various loads can be observed in Figure 12. The data displays that the efficiency is high and the operating range is large, both when charging and discharging the battery.

Figure 13 shows the DC-link voltage response of the proposed system. With a reference DC-link voltage of 180 V, the output voltage reaches approximately 195 V under steady-state conditions, resulting in a 15 V steady-state error. This response is used to evaluate the voltage regulation performance of the proposed PID-based control strategy. Figure 14 examines the battery power in use when the device is in various operating modes. Positive battery power is associated with the charging operation, and a negative one results in discharging, which proves appropriate management of power flow in both directions.

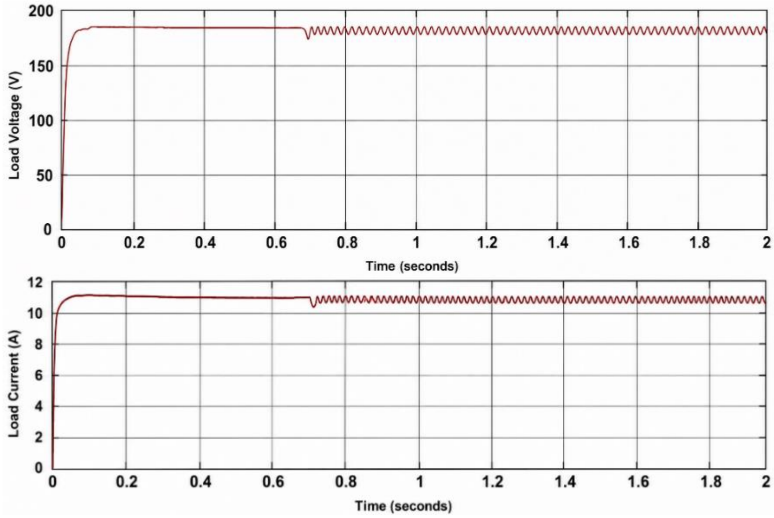

Figure 6. Analysis of load voltage and current response of the proposed converter

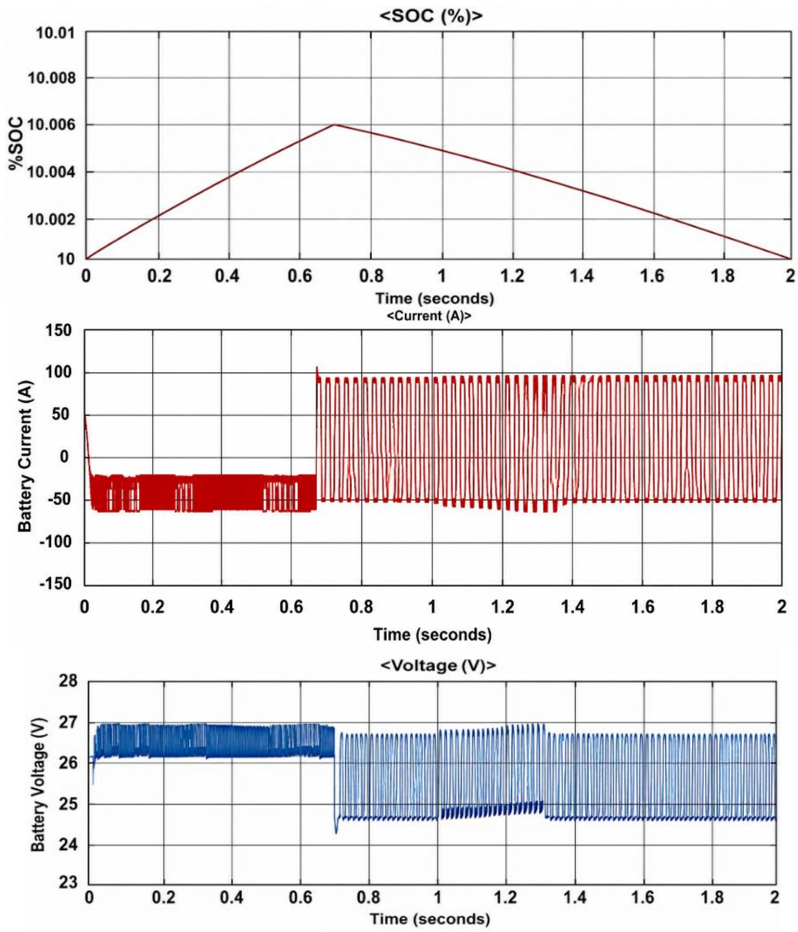

Figure 7. Analysis of battery SoC during PV charging and battery discharging

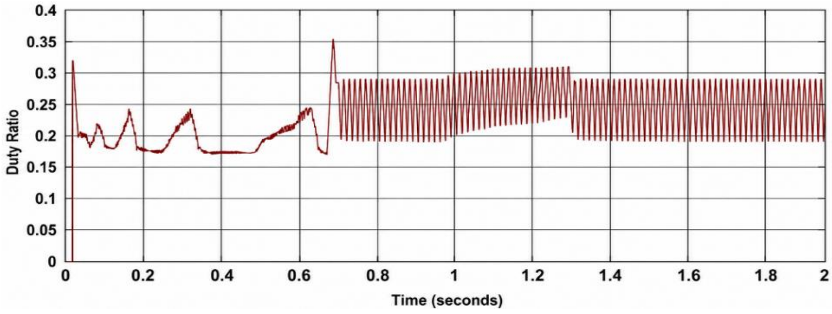

Figure 8. Analysis of duty ratio variation with changes in solar irradiation

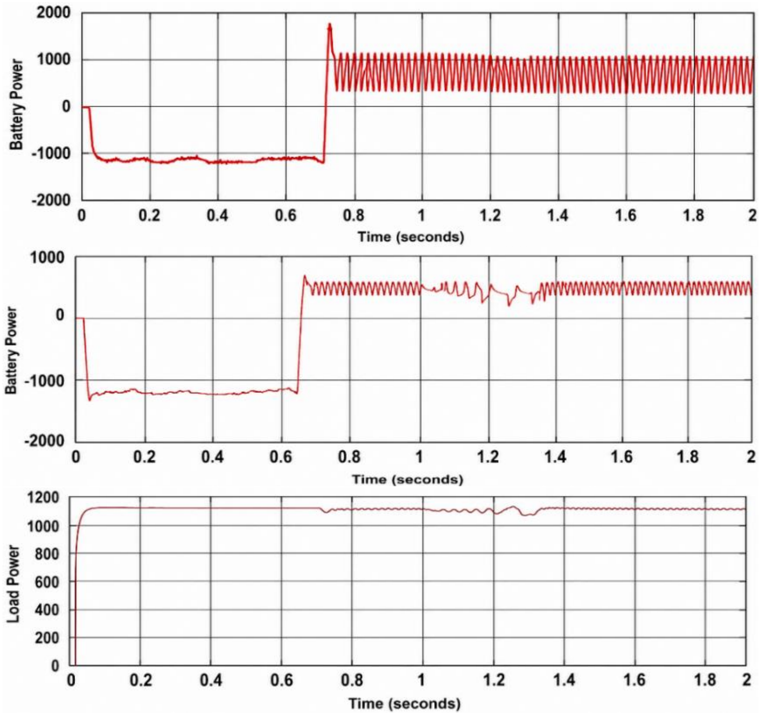

Figure 9. Analysis of power sharing among the PV source, battery, and load

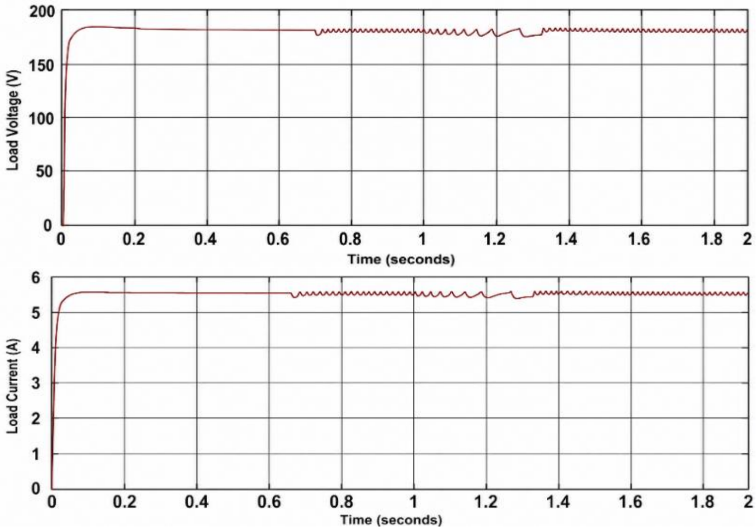

Figure 10. Analysis of load voltage and current under varying load conditions

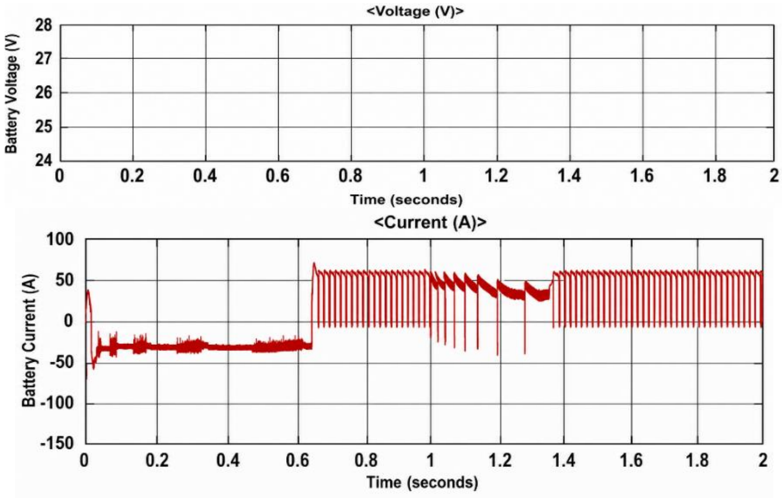

Figure 11. Analysis of battery voltage and current during charging and discharging

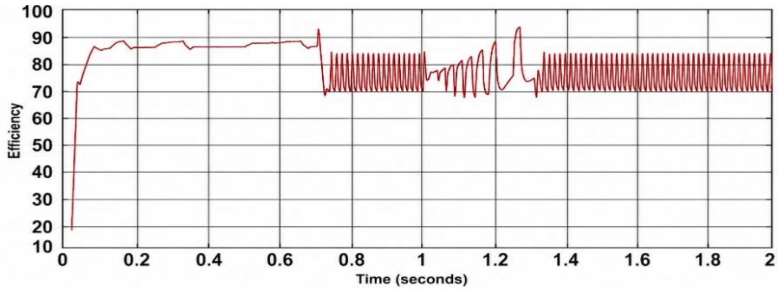

Figure 12. Analysis of converter efficiency under different load conditions

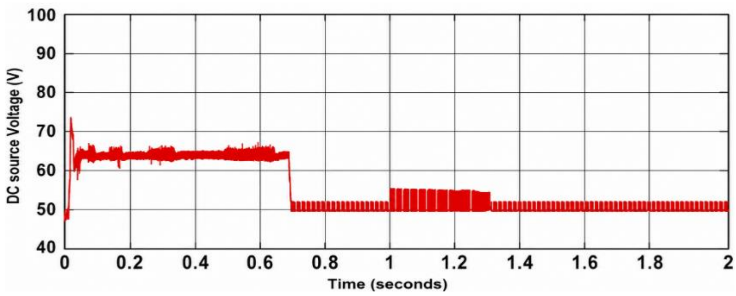

Figure 13. Analysis of DC-link voltage response of the proposed system

From Tables 1 and 2, it is observed that there is not much variation in the rise time for different loading conditions. Settling time is increasing as the power factor decreases. Steady state error is decreasing as the load increases in the power factor. It is observed that efficiency for higher load decreases, and also decreases in efficiency as the power factor decreases.

Table 1. Comparison of bidirectional buck-boost converter parameters for different power ratings

Parameter		Rise time (s)	Settling time (s)	Steady state error (V)
1 kW		0.021	0.0415	1.7
2 kW		0.032	0.059	1.35
	PF1	0.01	0.025	0.8
5 kW	PF0.9	0.01	0.046	5.6
	PF0.8	0.01	0.0815	5.65
	PF0.7	0.014	0.09	6.1

Table 2. Comparison of bidirectional buck-boost converter parameters for different power ratings are efficiency

Parameter		Battery power (W) Charge	Discharge	Input power (W)	Load power (W)	Efficiency (%)
1 kW		500	250	842	776.5	91
2 kW		350	400	2780	2420	87.13
5 kW	PF 1.0	680	5000	6420	5650	87.85
	PF 0.9	450	4260	5365	4620	84.54
	PF 0.8	460	4320	5365	4517	82.66
	PF 0.7	460	4300	5366	4414	80.7

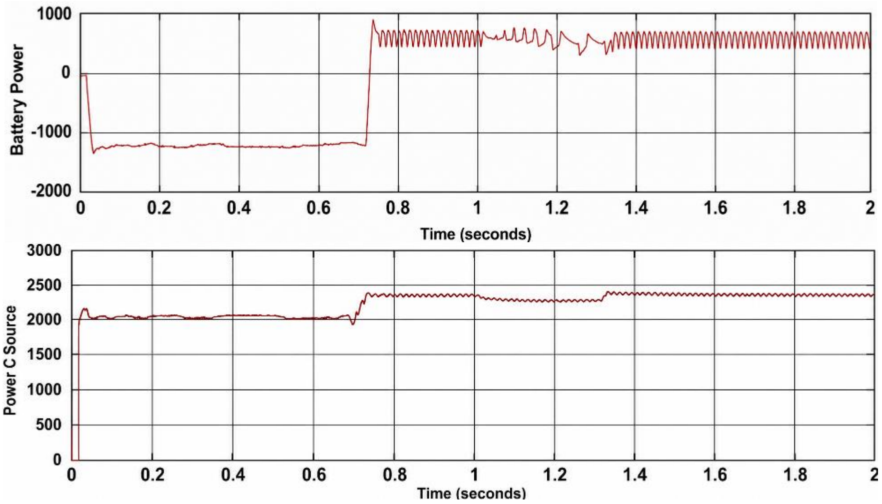

Figure 14. Analysis of battery power during different operating modes

6. CONCLUSION

A four-port bidirectional buck-boost converter with a PID controller is designed, and a simulation is carried out using MATLAB/Simulink. The P&O algorithm is implemented for optimal tracking of solar radiation. Simulation is carried out for different loads with different power factors. For each case, efficiency is calculated results indicate that this module can able to feed the uninterrupted power supply to the load up to 5 kW with acceptable efficiency, with a difficult power factor.

FUNDING INFORMATION

This research did not receive any specific grant from funding agencies in the public, commercial, or not-for-profit sectors.

AUTHOR CONTRIBUTIONS STATEMENT

This journal uses the Contributor Roles Taxonomy (CRediT) to recognize individual author contributions, reduce authorship disputes, and facilitate collaboration.

Name of Author	C	M	So	Va	Fo	I	R	D	O	E	Vi	Su	P	Fu
M. S. Mukundaswamy	✓	✓	✓		✓	✓		✓	✓	✓	✓		✓	
Smitha Elsa Peter	✓	✓		✓		✓		✓	✓	✓	✓	✓	✓	

C : **C**onceptualization
M : **M**ethodology
So : **So**ftware
Va : **Va**lidation
Fo : **Fo**rmal analysis
I : **I**nvestigation
R : **R**esources
D : **D**ata Curation
O : Writing - **O**riginal Draft
E : Writing - Review & **E**diting
Vi : **Vi**sualization
Su : **Su**pervision
P : **P**roject administration
Fu : **Fu**nding acquisition

CONFLICT OF INTEREST STATEMENT

Authors state no conflict of interest.

DATA AVAILABILITY

Data availability is not applicable to this paper as no new data were created or analyzed in this study.

REFERENCES

[1] Y. Sato, H. Nagata, and M. Uno, "Non-isolated multi-port converter integrating PWM and phase-shift converters," in *TENCON 2017 - 2017 IEEE Region 10 Conference*, Nov. 2017, pp. 1097–1102. doi: 10.1109/TENCON.2017.8228021.

[2] S. Venkataraman, C. Ziesler, P. Johnson, and S. Van Kempen, "Integrated wind, solar, and energy storage: Designing plants with a better generation profile and lower overall cost," *IEEE Power and Energy Magazine*, vol. 16, no. 3, pp. 74–83, May 2018, doi: 10.1109/MPE.2018.2793478.

[3] A. K. Bhattacharjee and I. Batarseh, "An interleaved boost and dual active bridge-based single-stage three-port DC–DC–AC Converter With Sine PWM Modulation," *IEEE Transactions on Industrial Electronics*, vol. 68, no. 6, pp. 4790–4800, Jun. 2021, doi: 10.1109/TIE.2020.2992956.

[4] J. Zhang *et al.*, "A three-port LLC resonant DC/DC converter," *IEEE Journal of Emerging and Selected Topics in Power Electronics*, vol. 7, no. 4, pp. 2513–2524, Dec. 2019, doi: 10.1109/JESTPE.2019.2902425.

[5] J. Zeng, J. Ning, X. Du, T. Kim, Z. Yang, and V. Winstead, "A four-port DC-DC converter for a standalone wind and solar energy system," *IEEE Transactions on Industry Applications*, pp. 1–1, 2019, doi: 10.1109/TIA.2019.2948125.

[6] P. Prabhakaran and V. Agarwal, "Novel four-port DC–DC converter for interfacing solar PV–fuel cell hybrid sources with low-voltage bipolar DC microgrids," *IEEE Journal of Emerging and Selected Topics in Power Electronics*, vol. 8, no. 2, pp. 1330–1340, Jun. 2020, doi: 10.1109/JESTPE.2018.2885613.

[7] S. Sharma, K. Rajambal, and C. Kalaivani, "Modelling of four-port converter for electric vehicle applications," *Journal of Energy Engineering and Thermodynamics*, no. 25, pp. 1–19, Sep. 2022, doi: 10.55529/jeet.25.1.19.

[8] T. Chaudhury and D. Kastha, "A high gain multiport DC–DC converter for integrating energy storage devices to DC microgrid," *IEEE Transactions on Power Electronics*, vol. 35, no. 10, pp. 10501–10514, Oct. 2020, doi: 10.1109/TPEL.2020.2977909.

[9] P. Kolahian, H. Tarzamni, A. Nikafrooz, and M. Hamzeh, "Multi-port DC–DC converter for bipolar medium voltage DC micro-grid applications," *IET Power Electronics*, vol. 12, no. 7, pp. 1841–1849, Jun. 2019, doi: 10.1049/iet-pel.2018.6031.

[10] Y. Liang, "Parallel coordination control of multi-port DC-DC converter for stand-alone photovoltaic-energy storage systems," *CPSS Transactions on Power Electronics and Applications*, vol. 5, no. 3, pp. 235–241, Sep. 2020, doi: 10.24295/CPSSTPEA.2020.00020.

[11] X. Du, J. Zeng, J. Ning, T. Kim, and V. Winstead, "Modeling and control of a four-port DC-DC converter for a DC microgrid with renewable energy sources," in *2020 IEEE Applied Power Electronics Conference and Exposition (APEC)*, Mar. 2020, pp. 3391–3396. doi: 10.1109/APEC39645.2020.9124276.

[12] N. D. Dao, D.-C. Lee, and Q. D. Phan, "High-efficiency SiC-based isolated three-port DC/DC converters for hybrid charging stations," *IEEE Transactions on Power Electronics*, vol. 35, no. 10, pp. 10455–10465, Oct. 2020, doi: 10.1109/TPEL.2020.2975124.

[13] F. S. Dinniyah, W. Wahab, and M. Alif, "Simulation of buck-boost converter for solar panels using PID controller," *Energy Procedia*, vol. 115, pp. 102–113, Jun. 2017, doi: 10.1016/j.egypro.2017.05.011.

[14] K. F. Hussein, I. Abdel-Qader, and M. K. Hussain, "Hybrid fuzzy PID controller for buck-boost converter in solar energy-battery systems," in *2015 IEEE International Conference on Electro/Information Technology (EIT)*, May 2015, pp. 070–075. doi: 10.1109/EIT.2015.7293323.

[15] K. Ramireddy, Y. Hirpara, and Y. V. Pavan Kumar, "Transient performance analysis of buck boost converter using various PID gain tuning methods," in *2020 12th International Conference on Computational Intelligence and Communication Networks (CICN)*, Sep. 2020, pp. 321–326. doi: 10.1109/CICN49253.2020.9242557.

[16] K. Sharma and D. K. Palwalia, "Design of digital PID controller for voltage mode control of DC-DC converters," in *2017 International conference on Microelectronic Devices, Circuits and Systems (ICMDCS)*, Aug. 2017, pp. 1–6. doi: 10.1109/ICMDCS.2017.8211715.

[17] P. Sabarish, R. Karthick, A. Sindhu, and N. Sathiyanathan, "Investigation on performance of solar photovoltaic fed hybrid semi impedance source converters," *Materials Today: Proceedings*, vol. 45, pp. 1597–1602, 2021, doi: 10.1016/j.matpr.2020.08.390..

[18] P. Azer and A. Emadi, "Generalized state space average model for multi-phase interleaved buck, boost and buck-boost DC-DC converters: transient, steady-state and switching dynamics," *IEEE Access*, vol. 8, pp. 77735–77745, 2020, doi: 10.1109/ACCESS.2020.2987277.

[19] A. R. Ulhe and V. V. Kulkarni, "PID control based boost converter for renewable power source," *International Journal of Engineering Research and*, vol. V9, no. 08, Aug. 2020, doi: 10.17577/IJERTV9IS080157.

[20] B. Patel, J. Patel, and U. Wani, "A new active power factor correction," pp. 6927–6934, 2016, doi: 10.15680/IJIRSET.2016.0505044.

[21] J.-K. Han, J.-I. Baek, Y. Jeong, C.-O. Yeon, and G.-W. Moon, "A simple THD improving method for CCM boost PFC converter under mixed conduction mode operation," in *2017 IEEE 3rd International Future Energy Electronics Conference and ECCE Asia (IFEEC 2017 - ECCE Asia)*, Jun. 2017, pp. 466–470. doi: 10.1109/IFEEC.2017.7992083.

[22] K. Kumar Jha, B. Mahato, P. Prakash, and K. Chandra Jana, "hardware implementation of single phase power factor correction system using micro-controller," *International Journal of Power Electronics and Drive Systems (IJPEDS)*, vol. 7, no. 3, p. 790, Sep. 2016, doi: 10.11591/ijpeds.v7.i3.pp790-799.

[23] A. A. Aleem and P. V. S. Ponkshe, "Adaptive approach for reducing the total harmonic distortion of boost converter using PWM switching," pp. 1229–1232, 2019.

[24] A. M. Fuad, M. A. M. Oninda, N. M. Muntasir, and Nafiul Islam, "Design and simulation of a DC - DC boost converter with PID controller for enhanced performance," *International Journal of Engineering Research and Technology*, vol. V6, no. 09, Sep. 2017, doi: 10.17577/IJERTV6IS090029.

[25] M. Shabeeh and A. Thakur, "Reduction in total - harmonic- distortion for AC To DC converter with improved power factor using boost converter with PID controller," *International Journal of Advance Research and Innovative Ideas in Education*, vol. 5, no. 4, pp. 411–421, 2019, [Online]. Available: https://h1.nu/1ptRm.

[26] M. Asim, H. Parveen, M. M.A., and A. Siddiqui, "Performance evaluation of PFC boost converters," *IJIREEICE*, vol. 3, no. 11, pp. 107–110, Nov. 2015, doi: 10.17148/IJIREEICE.2015.31122.

[27] D. K. Sah, N. Mazumdar, P. Pal, and T. Amgoth, "A comprehensive study of solar energy harvesting system in wireless sensor networks," in *2022 IEEE 9th Uttar Pradesh Section International Conference on Electrical, Electronics and Computer Engineering (UPCON)*, Dec. 2022, pp. 1–6. doi: 10.1109/UPCON56432.2022.9986433.

[28] A. R. Kalaiarasi, M. Dharani, A. J. Josphin, and A. Rithubarnika, "A review on error reduction in a closed-loop buck-boost converter through the implementation of different controllers," in *2024 International Conference on IoT Based Control Networks and Intelligent Systems (ICICNIS)*, Dec. 2024, pp. 677–683. doi: 10.1109/ICICNIS64247.2024.10823340.

[29] K. Paramasivam, R. Kavitha, P. Maithili, S. Poojavarshini, N. S. Vaani, and K. G. S. Dev, "Design and realization of voltage lift luo converter with PID controller for solar power," in *2023 2nd International Conference on Advancements in Electrical, Electronics, Communication, Computing and Automation (ICAECA)*, Jun. 2023, pp. 1–6. doi: 10.1109/ICAECA56562.2023.10199217.

BIOGRAPHIES OF AUTHORS

M. S. Mukundaswamy was born in Mandya (Taluk), Mandya (District), Karnataka, India on May 01 1978, received a bachelor's degree in electrical and electronics engineering from Mysuru University in March 2003, an M.E. degree in VLSI design and embedded systems from Visvesvaraya Technological University (VTU) in 2014, and a Ph.D. Degree (in the field of electronics department) from PRIST University, Tanjavur, India in 2024. Currently working as an assistant professor in the Department of Electrical and Electronics Engineering at Dr. AIT Bengaluru, India. His research areas include power electronics. He can be contacted at email: mukundswamyms.ee@drait.edu.in.

Smitha Elsa Peter has been working as a professor in the Department of Electronics and Communication Engineering at Ponnaiyah Ramajayam Institute of Science ansd Technology (PRIST) Deemed to be University for the past 17 years. She completed her bachelor's in engineering from the University of Madras in 2001 and masters in engineering. (applied electronics) from Karunya University in 2006. She completed her Doctor of Philosophy in the Department of Electronics and Communication Engineering from PRIST University in 2016. She has published more than 20 journal papers in reputed journals. Her research interests include image processing, soft computing, machine learning techniques, and deep learning. She can be contacted at email: smithasishaj@gmail.com.